SI part

Detection of the ferroelectric order in new magnetic coordination networks.

P. Farger,[a#] C. Leuvrey,[a] M. Lenertz,[a] G. Taupier,[a] K. D. Dorkenoo,[a] D. Ihiawakrim,[a] S. Cherifi-Hertel,[a] G. Rogez,[a] P. Rabu,[a] E. Delahaye[a§]

[a.] Université de Strasbourg, CNRS, Institut de Physique et Chimie des Matériaux de Strasbourg, UMR 7504, 67034 Strasbourg, France.

[&.] Present address: Synthèse Caractérisation ANalyse de la MATière (ScanMAT) - UAR CNRS 2025, Université de Rennes 1, Beaulieu - Bâtiment 10A, 263 avenue du Général Leclerc, 35042 Rennes, France

[#.] Present address: CNRS, Laboratoire de Chimie de Coordination, 205 route de Narbonne, 31077 Toulouse, France and Université de Toulouse, UPS, INPT, LCC, 31077 Toulouse, France.

SEM Analysis

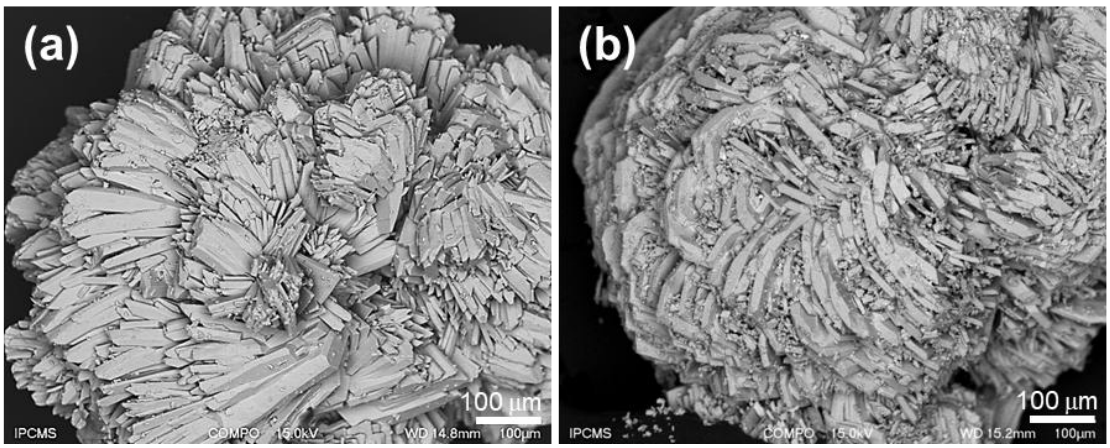

Figure S1. SEM images in composition for the compounds **(a) $[Gd_2(L^*)_2(ox)_2(H_2O)_2]$** and **(b) $[Dy_2(L^*)_2(ox)_2(H_2O)_2]$**.

Crystal Structure

The imidazolium dicarboxylate ligand L (non chiral) and L* (chiral) are represented in the scheme S1.

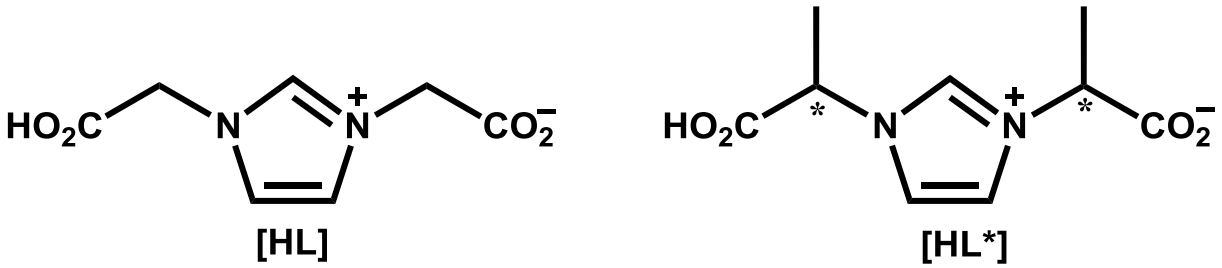

Scheme S1. Representation of the imidazolium dicarboxylate ligands L and L*, in their protonated form, used in this work.

The crystal structures of the title compound **[$Dy_2(L^*)_2(ox)_2(H_2O)_2$]** is iso-structural with that of the Gd compound **[$Gd_2(L^*)_2(ox)_2(H_2O)_2$]**. The corresponding CIF file has been deposited as CCDC 2160787. [1] For comparison the CIF file of the non polar analogue **[$Gd_2(L)_2(ox)_2(H_2O)_2$]** was deposited as CCDC 1541843.[2]

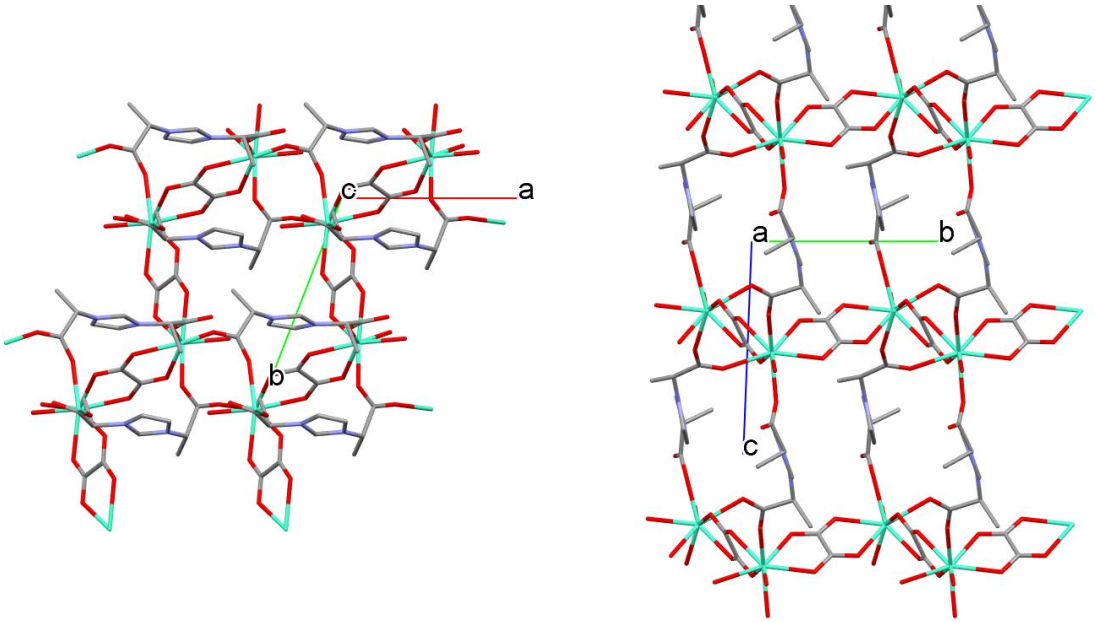

Figure S2. Representations of the 3D network for **[$Gd_2(L^*)_2(ox)_2(H_2O)_2$]** (Gd in green, C in grey, O in red, N in blue) along ***c*** (left) and along ***a*** (right), showing interconnection between Gd^{3+} chains through the L* ligands. After the CIF file deposited as CCDC 2160787. [1]

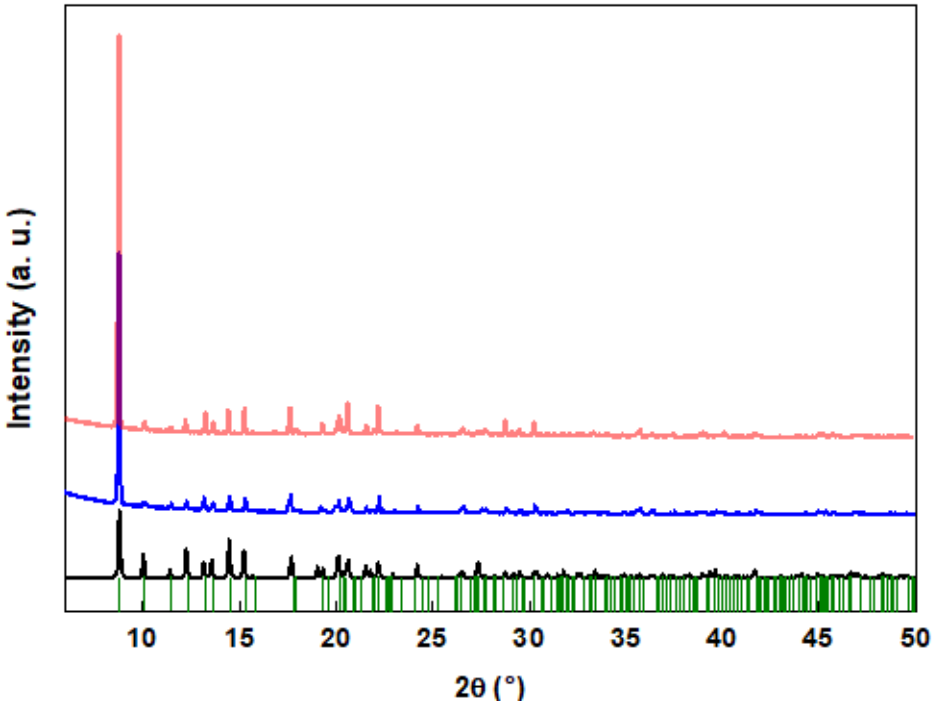

Figure S3. Comparison of the experimental X-ray powder pattern for the compounds **$[Gd_2(L^*)_2(ox)_2(H_2O)_2]$** (blue line) and **$[Dy_2(L^*)_2(ox)_2(H_2O)_2]$** (pink line) to the calculated pattern from the single crystals X-ray data for the compound **$[Gd_2(L^*)_2(ox)_2(H_2O)_2]$** (black line).

TG and Temperature solved PXRD Analysis

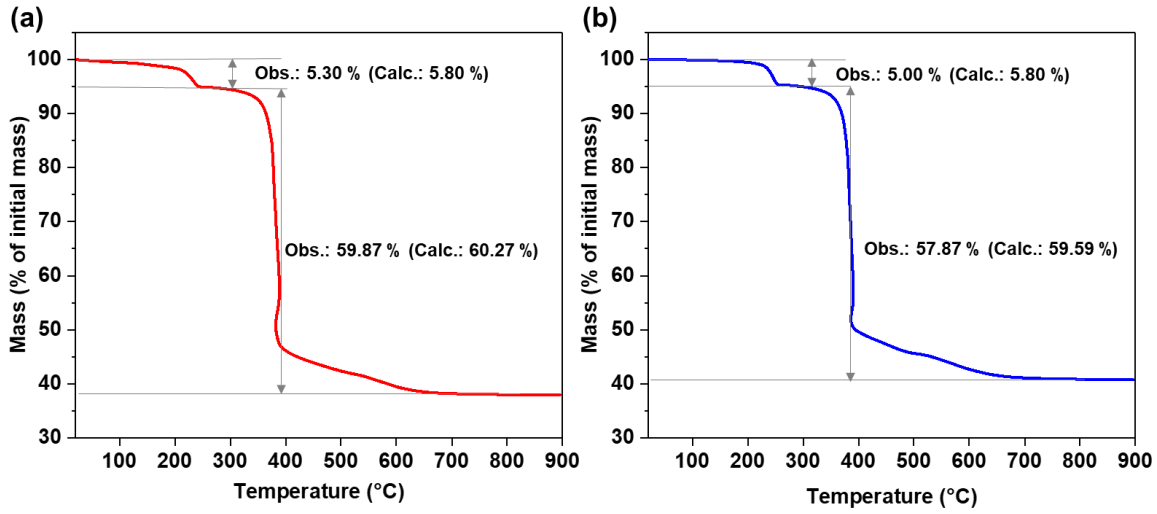

Figure S4. Thermogravimetric analysis under air with a heating rate of 5°C/min of the compounds **(a) $[Gd_2(L^*)_2(ox)_2(H_2O)_2]$** (red line) and **(b) $[Dy_2(L^*)_2(ox)_2(H_2O)_2]$** (blue line).

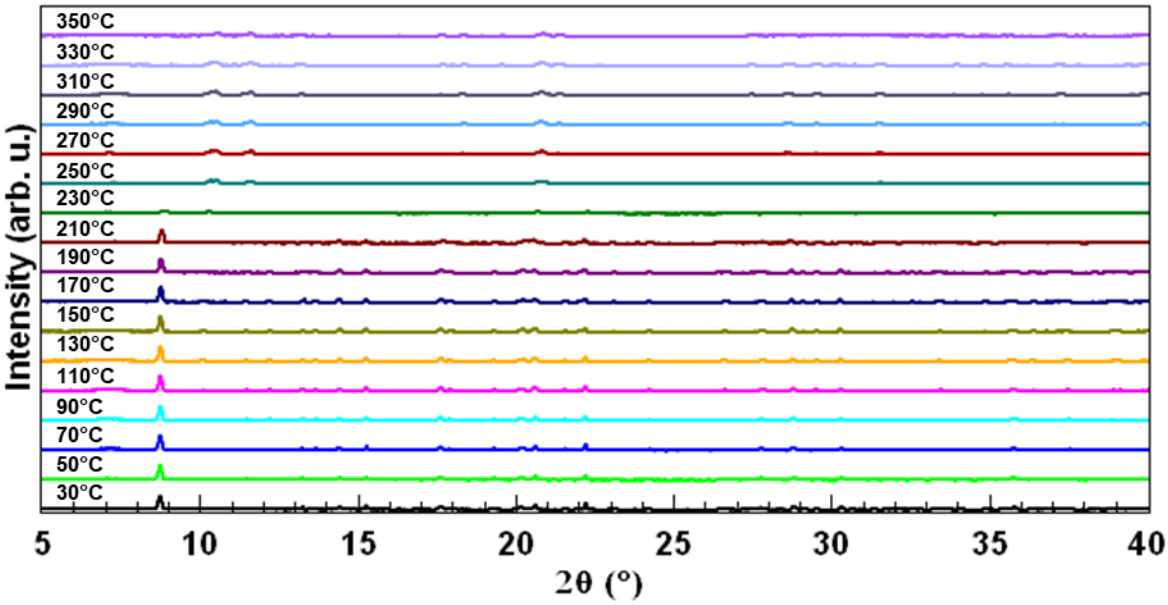

Figure S5. Thermal variation under air of the PXRD pattern of **$[Dy_2(L^*)_2(ox)_2(H_2O)_2]$** from T = 30°C to T = 350°C with a step of 20°C (3h/scan). The patterns were recorded with variable slit for constant illumination of 3 mm, without intensity correction for better visibility.)

Composition by SEM

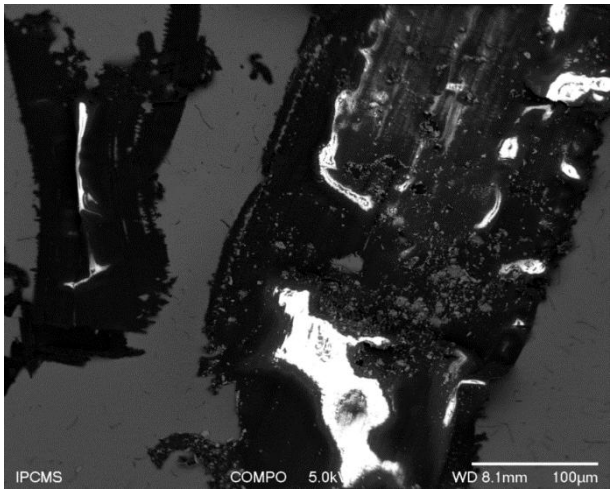

Figure S6. SEM image in composition of the slices of resin incorporating the compound **$[Gd_2(L^*)_2(ox)_2(H_2O)_2]$**.

SEM images in composition show the presence of **$[Gd_2(L^*)_2(ox)_2(H_2O)_2]$** crystals (in light grey) dispersed within the resin (in black). EDX analysis confirms the presence of Gd in the light grey areas.

These observations indicate that the integrity of **[$Gd_2(L^*)_2(ox)_2(H_2O)_2$]** is conserved after embedded in resin.

Dielectric measurements

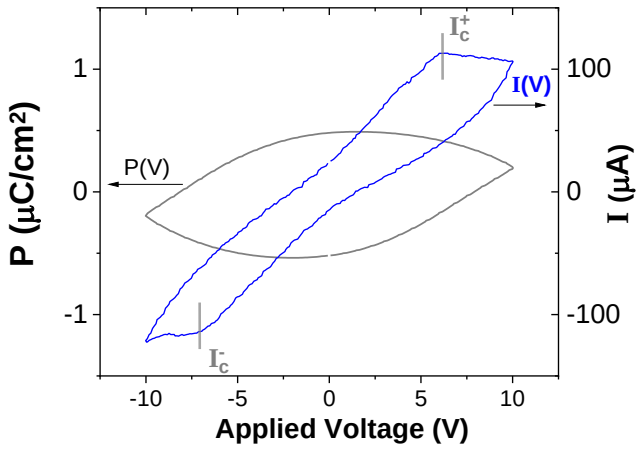

Figure S7. Dynamic P(V) and the corresponding I(V) measured at a voltage sweep frequency of 1 kHz. The P(V) curve is a minor loop in our recording conditions. Moreover, the sample thickness was roughly evaluated, which contributes to uncertainty on the coercive electric field value in the P(V) curve.

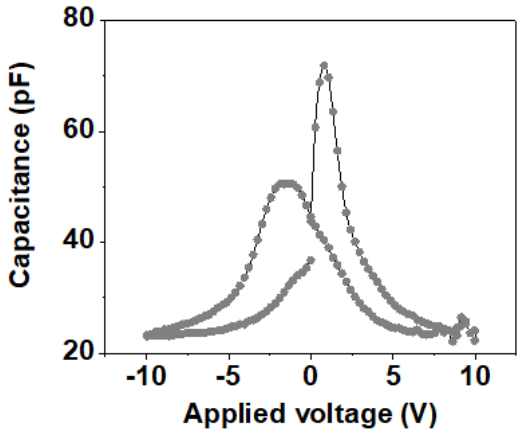

Figure S8. Static capacitance response of **[$Dy_2(L^*)_2(ox)_2(H_2O)_2$]** embedded in resin to a DC bias voltage superposed to a small excitation voltage (1-2 V at 200 Hz). It worth noticing that the capacitance measured in this compound cannot be quantitatively compared to that measured in **[$Dy_2(L^*)_2(ox)_2(H_2O)_2$]** since the size (surface and thickness) of the two samples are different.

Figure S9. Photo obtained by stereomicroscope of the slices of resin incorporating **[$Gd_2(L^*)_2(ox)_2(H_2O)_2$]** deposited on the surface of the fixed copper electrode of the ferroelectric device.

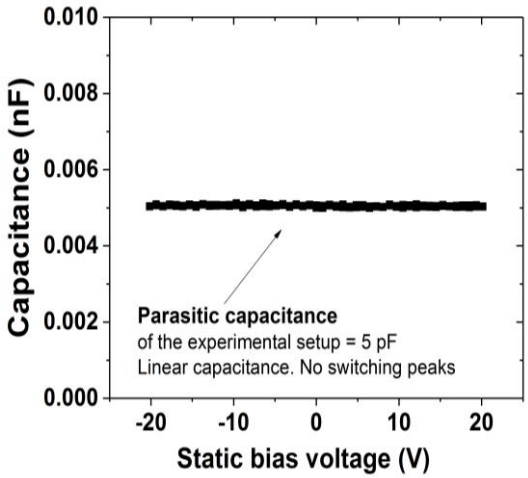

Figure S10. Curve of the parasitic capacitance induced by the experimental setup. It can be noticed that the capacitance shows a linear response with the applied voltage and that the capacitance value is negligible.

Magnetic data analysis

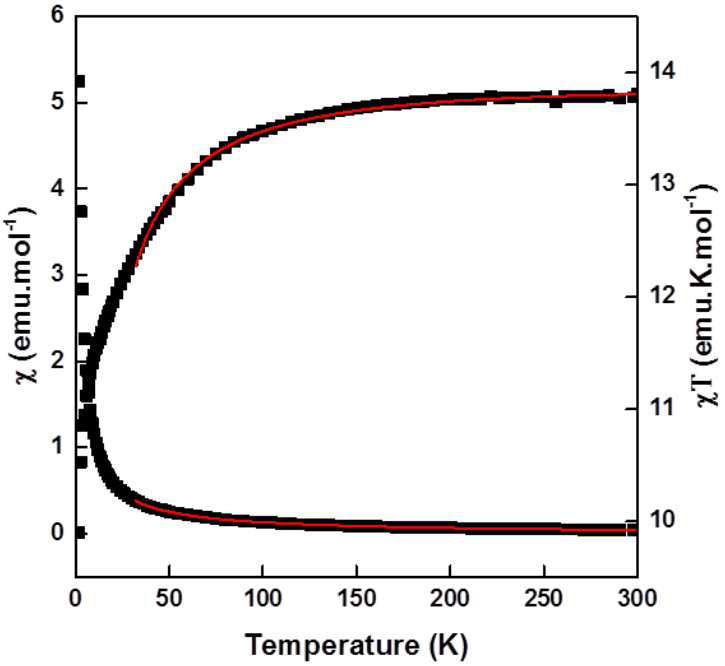

Figure S11. Plots of the magnetic susceptibility χ (open circles) and χT product (open squares) versus T for the compound **$[Dy_2(L^*)_2(ox)_2(H_2O)_2]$.** The full lines correspond to the best fit of the experimental data using the analytical expression for isolated ions given below.

The thermal variation of the magnetic susceptibility of $[Dy_2(L2)_2(ox)_2(H_2O)_2$has been fit with the following expression for Dy^{3+} ions :

$$\chi = \frac{Ng^2\beta^2}{kT} * \frac{0{,}5\exp\left(\frac{-0{,}25\Delta}{kT}\right) + 4{,}5\exp\left(\frac{-2{,}25\Delta}{kT}\right) + 12{,}5\exp\left(\frac{-6{,}25\Delta}{kT}\right) + 24{,}5\exp\left(\frac{-12{,}25\Delta}{kT}\right) + 40{,}5\exp\left(\frac{-20{,}25\Delta}{kT}\right) + 60{,}5\exp\left(\frac{-30{,}25\Delta}{kT}\right) + 84{,}5\exp\left(\frac{-42{,}25\Delta}{kT}\right) + 112{,}5\exp\left(\frac{-56{,}25\Delta}{kT}\right)}{1 + 2\exp\left(\frac{-0{,}25\Delta}{kT}\right) + 2\exp\left(\frac{-2{,}25\Delta}{kT}\right) + 2\exp\left(\frac{-6{,}25\Delta}{kT}\right) + 2\exp\left(\frac{-12{,}25\Delta}{kT}\right) + 2\exp\left(\frac{-20{,}25\Delta}{kT}\right) + 2\exp\left(\frac{-30{,}25\Delta}{kT}\right) + 2\exp\left(\frac{-42{,}25\Delta}{kT}\right) + 2\exp\left(\frac{-56{,}25\Delta}{kT}\right)}$$

with *N* the Avogadro constant, *g* the Zeeman factor, *k* the Boltzmann contant, β the Bohr magneton and Δ the ZFS parameter. The refined value for $[Dy_2(L2)_2(ox)_2(H_2O)_2]$ is Δ = 0,237(3) cm^{-1}.[3]

REFERENCES

[1] T. Ekanayaka, T. Jiang, E. Delahaye, O. Perez, J.-P. Sutter, D. Le, A. T. N'Diaye, R. Streubel, T. S. Rahman, P. A. Dowben, *Phys. Chem. Chem. Phys.* **2023**, *25*, 6416–6423.
[2] P. Farger, C. Leuvrey, M. Gallart, P. Gilliot, G. Rogez, J. Rocha, D. Ananias, P. Rabu, E. Delahaye, *Beilstein J. Nanotechnol.* **2018**, *9*, 2775–2787.
[3] J. Cepeda, R. Balda, G. Beobide, O. Castillo, J. Fernández, A. Luque, S. Pérez-Yáñez, P. Román, *Inorg. Chem.* **2012**, *51*, 7875–7888.